(Received 16 May 2024, Accepted 11 October 2024, Scheduled 17 October 2024)

Three-Phase Duty Cycle Modulation-Based Model Predictive Control Strategy for QZSI-PMSM System without Cost Function

Yang Zhang[1], Kun Cao[1], Wenjing Yi[1], Yuwei Meng[1], and Zhun Cheng[2,*]

[1]*Hunan University of Technology, Zhuzhou 412007, China*
[2]*Hunan Railway Professional Technology College, Zhuzhou 412001, China*

ABSTRACT: The finite set model predictive control (FCS-MPC) method for quasi-Z-source inverter-permanent magnet synchronous motor (QZSI-PMSM) system suffers from the problems of unclear linkage between control objectives, complex control system, and poor control performance. A three-phase duty cycle modulation-based model predictive control (TDCM-MPC) strategy without cost function is proposed. In this strategy, the control objectives are converted firstly to make a connection between the control variables of inverter-side and motor-side, and based on it construct a system of nonhomogeneous linear equations to calculate the three-phase duty cycle. In addition, the three-phase duty cycles may have a secondary correction according to the size of the capacitor voltage error to realize the overall control of the four control variables. Finally, the driving pulse is generated based on space vector modulation (SVM) to obtain smaller steady-state ripples. The experimental results show that, compared with the conventional FCS-MPC, the proposed TDCM-MPC strategy reduces the computation of the control system and can obtain better control performance.

1. INTRODUCTION

Z-source inverter (ZSI) is a new power conversion topology with a straight-through (ST) state. This state is able to realize the boost function, which overcomes the limitation of conventional voltage source inverters that can only realize the buck function [1], and it does not need to take into account the effect of the dead time of the switching devices on the output effect of the inverter. Quasi-Z-source inverter (QZSI) inherits the characteristics of ZSI, and it has continuous input current, which improves the practicality of the inverter [2, 3]. Based on the above advantages, QZSI has been used and developed widely in wind power generation, photovoltaic power generation, and hybrid vehicles [4–6].

Model predictive control (MPC) uses a mathematical model to predict the future behavior of the system and designs a cost function about the error of multiple control variables to find the optimal action [7]. It is widely used in areas such as power electronics and motor drives due to its ability to handle nonlinearities and complex constraints [8–12]. Currently, the application of MPC to PMSM control systems has received great attention. In [13, 14], the selection range of voltage vectors (VVs) is extended to minimize the steady-state ripple of output current. In [15], the reference voltage vector containing motor speed and current information is predicted based on the deadbeat control principle. The weighting factor is avoided because only the error of voltage vector is included in the cost function. In order to reduce the number of predictions, a method for fast screening of voltage vectors is used in [16], and a duty cycle modulation method is proposed in [17]. In [18], parameter identification method is combined with MPC to enhance the robustness of the system.

Some scholars attempted to optimize the application of MPC to QZSI by reducing the weight coefficients and the number of predictions of MPC [19]. Ref. [20] proposes to determine whether to use an ST vector in the next control cycle based on the predicted value of inductor current, removing the item of inductor current error from the cost function. In [21], an error ranking method based on logic operations is devised to eliminate all the weighting coefficients. In [22, 23], a sequential-MPC (S-MPC) method is proposed to eliminate some or all of the weighting coefficients. In [24], an ST VV, a zero VV, and an effective VV are used as joint voltage vector in one control cycle to obtain better steady state results. However, the authors did not consider the effect of increased switching frequency on the system. Ref. [25] proposes a QZSI predictive control method based on a discrete time averaging model, which does not require cost function estimation, weight factor selection, or proportional-integral (PI) parameter design.

Applying MPC approach to a QZSI-PMSM drive system is even more challenging due to the unclear connection between its control objectives. Ref. [26] uses two independent MMPC loops for ZSI and PMSM control and suppresses the steady-state ripple of control variables effectively by vector modulation. However, the control quantities generated by the two control loops may have conflict because the control variables on the two sides are independent of each other. In [27], the unified control of the inverter side and motor side in QZSI-PMSM system is realized. However, the weight coefficients in its cost function are too many, and only one VV is applied in one control cycle, which cannot obtain a better steady-state effect. In [28], an effective VV or an ST VV is selected by the FCS-MPC algorithm, and the duty cycle of the candidate VV is calculated and synthesized with zero VV. The dynamic per-

* Corresponding author: Zhun Cheng (120277982@qq.com).

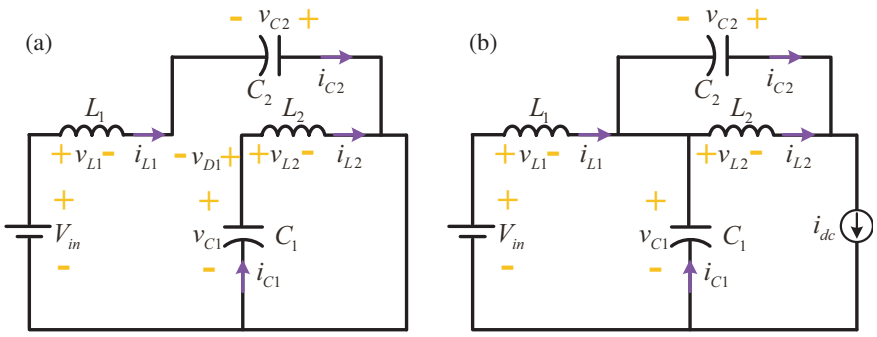

FIGURE 1. Two operating states of QZSI. (a) ST state. (b) NST state.

formance of the motor is improved, but it does not solve the problem of too many weight coefficients in the cost function. Ref. [29] adds an additional switching device to conventional quasi-Z-source topology and uses a two-stage ST VV to minimize torque fluctuations. However, this approach does not consider the performance of control variables on the QZSI side.

In this paper, a novel TDCM-MPC strategy is proposed for controlling all the control variables of a QZSI-PMSM system. Through the derivation of equations, the strategy concludes that the control of capacitor voltage on QZSI side can be equated to the control of DC bus current, and the control of output current on PMSM side can be equated to the control of the output voltage. In addition, a system of nonhomogeneous linear equations is constructed, which proves that it is impossible to realize the deadbeat control of the four control variables. The other methods must be proposed to minimize the overall output error of the system. The ST duty cycle and three-phase duty cycle are obtained by applying deadbeat control to the inductor current and output voltage, respectively. The three-phase duty cycle is corrected a second time when the error between the predicted and reference values of the capacitor voltage exceeds the correction threshold. This behavior sacrifices a small portion of the control accuracy for PMSM output current but realizes the overall control of the four control variables. The contributions of this paper can be summarized as follows:

1) Multiple non-straight-through (NST) VVs and an ST VV act alternately in a control cycle to generate driving pulses to reduce the steady-state ripple of capacitor voltage, inductor current, motor torque, and the THD of output current.

2) The control objectives of QZSI-PMSM system are converted equivalently to make a connection between the control variables on the QZSI side and PMSM side.

3) A system of nonhomogeneous linear equations is constructed to calculate the three-phase duty cycle directly without constructing a cost function or determining which sector the reference voltage vector is located. The control accuracy is improved while the computation of the control system is reduced greatly.

4) The three-phase duty cycles may have a secondary correction according to the size of the capacitor voltage error to realize the overall control of the four control variables.

2. QZSI-PMSM SYSTEM TOPOLOGY AND PREDICTION MODELING

In this section, the topology and prediction model of the QZSI-PMSM drive system will be presented. As shown in Fig. 3, the main circuit of this drive system consists of the following four components: a DC power supply, a quasi-Z source network, a three-phase inverter bridge, and a permanent magnet synchronous motor. Among them, the three-phase two-level inverter bridge and quasi-Z source network form the QZSI, which can provide voltage vectors with different effects. The DC power supply and PMSM serve as the energy input and output parts of the whole system, respectively.

2.1. Prediction Model of QZSI

The operating states of the quasi-Z source inverter can be categorized into straight-through (ST) state and non-straight-through (NST) state. The equivalent circuits of QZSI in these two states are shown in Fig. 1, where the two inductance and capacitance values are equal, i.e., $L_1 = L_2$ and $C_1 = C_2$, respectively.

When the QZSI operates in the ST state, as shown in Fig. 1(a), switch D_1 is disconnected; the power supply and capacitor C_2 charge inductor L_1; and capacitor C_1 discharges through inductor L_2. Under the premise of neglecting the inductor stray resistance, the state equations of inductor L_1 and capacitor C_1 can be expressed as:

$$\begin{cases} L_1 \frac{di_{L1}}{dt} = v_{C1} \\ C_1 \frac{dv_{C1}}{dt} = -i_{L1} \end{cases} \tag{1}$$

When the QZSI operates in the NST state, as shown in Fig. 1(b), switch D_1 is closed; the power supply and inductor L_1 charge capacitor C_1; and inductor L_2 charges capacitor C_2. Under the premise of neglecting the inductor stray resistance, the state equations of inductor L_1 and capacitor C_1 can be expressed as:

$$\begin{cases} L_1 \frac{di_{L1}}{dt} = V_{in} - v_{C1} \\ C_1 \frac{dv_{C1}}{dt} = i_{L1} - i_{dc} \end{cases} \tag{2}$$

where V_{in} is the power input voltage, and i_{dc} is the DC bus current, which is generally obtained from the switching state and output current of the three-phase inverter bridge.

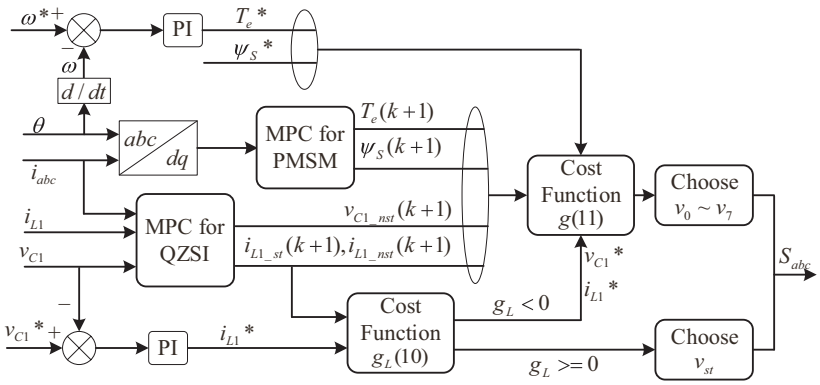

FIGURE 2. The block diagram of conventional FCS-MPC strategy.

As shown in Fig. 1, the equivalent circuits of QZSI in ST state and NST state are different, so the prediction models of v_{C1} and i_{L1} in the two operating states should be derived separately. The prediction model equations for i_{L1} and v_{C1} at the next moment are obtained using the first-order forward difference method as follows:

$$i_{L1}(k+1) = \begin{cases} i_{L1}(k) + \frac{T_S}{L_1} v_{C1}(k), \\ \qquad ST\ state \\ i_{L1}(k) + \frac{T_S}{L_1}[v_{in} - v_{C1}(k)], \\ \qquad NST\ state \end{cases} \tag{3}$$

$$v_{C1}(k+1) = \begin{cases} v_{C1}(k) + \frac{T_S}{C_1}[-i_{L1}(k+1)], \\ \qquad ST\ state \\ v_{C1}(k) + \frac{T_S}{C_1}[i_{L1}(k+1) - i_{dc}(k+1)], \\ \qquad NST\ state \end{cases} \tag{4}$$

where T_S is the control period, and $i_{dc}(k+1)$ is the DC bus current for the next control period, which can be obtained from the switching state of the three-phase inverter bridge in the next control period and the output current at the current moment:

$$i_{dc}(k+1) = S_a i_a + S_b i_b + S_c i_c \tag{5}$$

When the upper bridge arm of a phase is on and the lower bridge arm is off ($S_{xH} = 1, S_{xL} = 0, x = a, b, c$), the switching state of that phase is recorded as 1 ($S_x = 1, x = a, b, c$); when the upper bridge arm of a phase is off and the lower bridge arm is on ($S_{xH} = 0, S_{xL} = 1, x = a, b, c$), the switching state of that phase is recorded as 0 ($S_x = 1, x = a, b, c$).

2.2. Prediction Model of PMSM

In this paper, the surface-mounted PMSM is the object of study. The motor stator and rotor core reluctance are neglected; eddy current and hysteresis losses are not counted; the rotor has no damping winding; and the induced electromotive force in the stator winding is a sinusoidal wave. Under the two-phase rotating coordinate system, the voltage equation and magnetic chain equation of the PMSM can be expressed respectively as:

$$\begin{cases} v_d = R_s i_d - \omega_e \psi_q + L_d \frac{di_d}{dt} \\ v_q = R_s i_q + \omega_e \psi_d + L_q \frac{di_q}{dt} \end{cases} \tag{6}$$

$$\begin{cases} \psi_d = L_d i_d + \psi_f \\ \psi_q = L_q i_q \end{cases} \tag{7}$$

The electromagnetic torque equation is:

$$T_e = \frac{3}{2} p_n \psi_f i_q \tag{8}$$

where R_S, L_d, L_q, ψ_f, ω_e, v_d, v_q, i_d, i_q are stator resistance, the stator inductances of the d-q axis, permanent magnet flux linkage, electrical angular velocity, the voltages of the d-q axis, the currents of the d-q axis, respectively.

The motor speed can be regarded as an invariable value for a short time interval due to the slow change of mechanical quantities relative to electrical quantities. Applying first-order Eulerian discretization to (6), the prediction equation for the motor current during the following sampling period is represented as:

$$\begin{cases} i_d(k+1) = (1 - \frac{R_s T_s}{L_d}) i_d + \frac{T_s \omega_e L_q i_q}{L_d} + \frac{T_s v_d}{L_d} \\ i_q(k+1) = (1 - \frac{R_s T_s}{L_q}) i_q - \frac{T_s \omega_e (L_d i_d + \psi_f)}{L_q} + \frac{T_s v_q}{L_q} \end{cases} \tag{9}$$

3. TRADITIONAL FCS-MPC STRATEGY

The block diagram of conventional FCS-MPC strategy for QZSI-PMSM system is shown in Fig. 2. The reference value of the electromagnetic torque is generated through the speed PI loop, and the reference value of the inductor current is generated through the quasi-Z-source capacitor voltage PI loop.

The FCS-MPC strategy first determines whether the next cycle adopts the ST state based on the cost function g_L about the quasi-Z source inductor current [27]. If $g_L >= 0$, the ST VV is directly selected as the switching state in the next cycle; otherwise, the optimal VV is selected by calculating the cost function g including multiple control objectives such as capacitance voltage, inductance current, motor torque, and motor flux linkage. The NST VV corresponding to the smallest cost function is used as the switching state in the next cycle. The cost function for this strategy to determine whether to use the ST state can be defined as:

$$g_L = |i_{L1\_ref} - i_{L1\_nst}| - |i_{L1\_ref} - i_{L1\_st}| \tag{10}$$

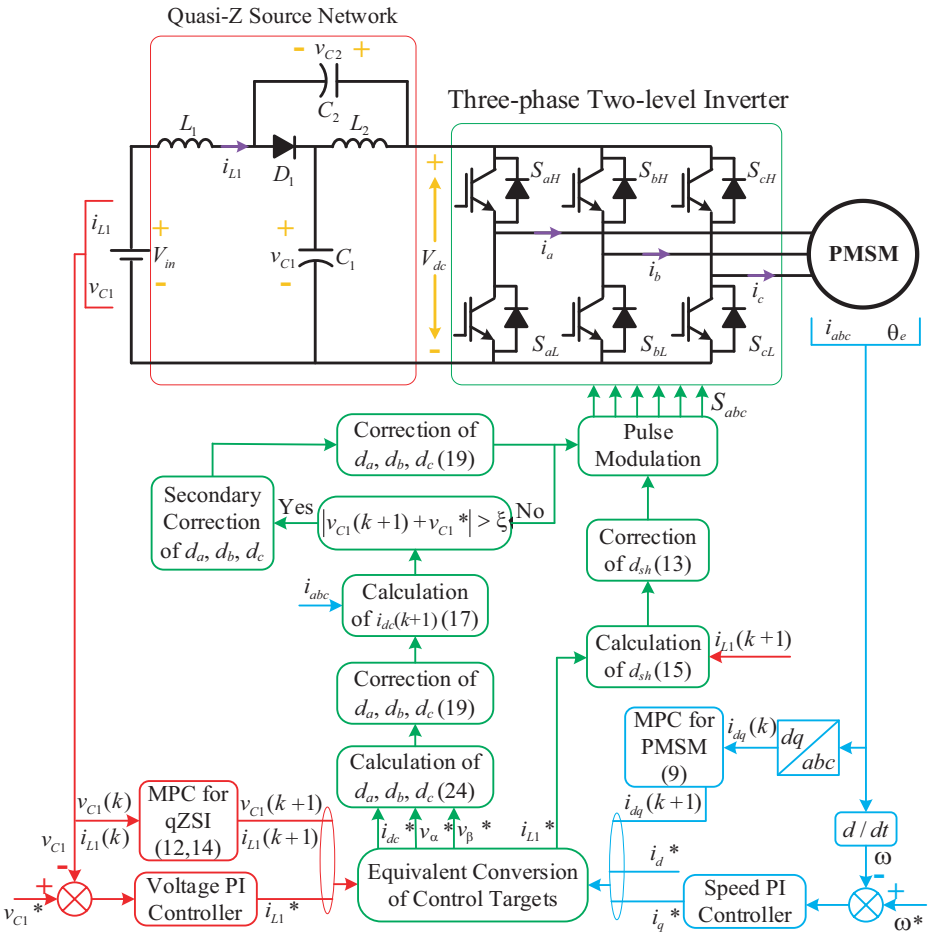

FIGURE 3. The block diagram of proposed TDCM-MPC strategy.

The multi-control objective cost function for this strategy can be defined as:

$$\begin{aligned} g \;=\; & |T_e* - T_e(k+1)| + Q_\psi\,|\psi_s* - \psi_s(k+1)| \\ & + Q_L\,|i_{L1\_ref} - i_{L1}(k+1)| \\ & + Q_C\,|v_{C1\_ref} - v_{C1}(k+1)| \end{aligned} \tag{11}$$

The cost function constructed by (11) has three weighting coefficients. However, there is no corresponding formula for the calculation of the weighting coefficients, which is generally obtained through several experimental verifications, and the size of the weighting coefficients will directly affect the system performance. This poses a great challenge to the design of the control system, and the behavior of optimization by using the cost function several times will also increase the computation of the control system.

4. PROPOSED TDCM-MPC STRATEGY

In order to reduce the computational amount of the control system of the traditional FCS-MPC strategy and realize the overall control of all control variables of a QZSI-PMSM system, a novel TDCM-MPC strategy is proposed in this paper. The method consists of four key components: the equivalent conversion of control objectives, the calculation and primary correction of the straight-through duty cycle and three-phase duty cycle, the secondary correction of the three-phase duty cycle based on the capacitor voltage prediction error, and the output of the driving pulse. The block diagram and detailed flow of proposed TDCM-MPC strategy is shown in Fig. 3.

4.1. The Equivalent Conversion of Control Objectives

The control objectives of the QZSI-PMSM system include inductor current (i_{L1}) and capacitor voltage (v_{C1}) on the inverter side, and d-axis current (i_d) and q-axis current (i_q) on the motor side. There seems to be no necessary connection between these control variables. Therefore, it is very necessary to perform equation derivation to find out the correlation between them.

The prediction equations of i_{L1} and v_{C1} are somewhat unique in that their predicted values will differ depending on the voltage vector applied. If the driving pulse is generated by alternating ST and NST VVs in one control cycle, the predicted value of i_{L1} in the next control cycle no longer satisfies (3). It can be assumed that i_{L1} varies linearly under the action of a single VV alone in the same control cycle, as shown in Fig. 4(a). Then, the predicted value of i_{L1} under the alternating action of multiple VVs can be obtained by summing up its changing

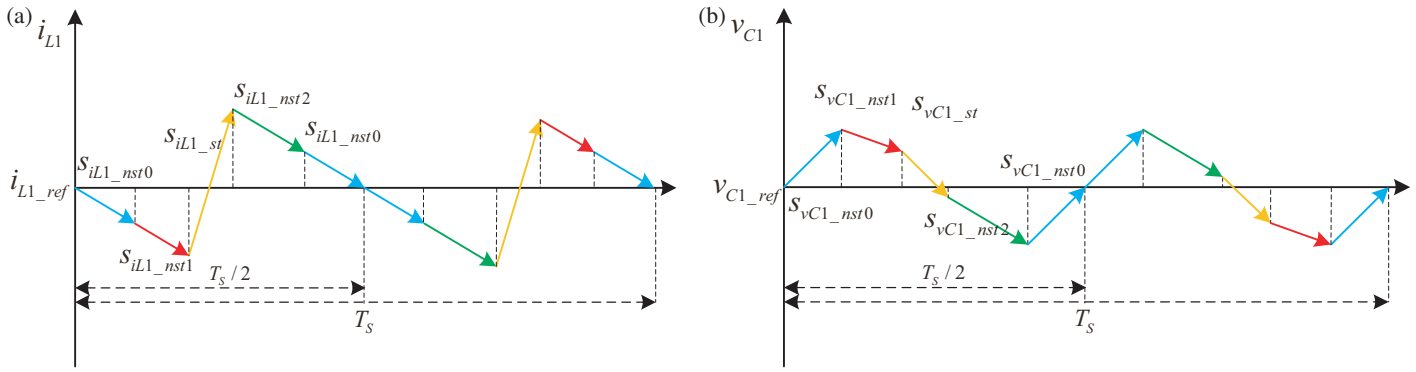

FIGURE 4. The effect of multiple VVs in one control cycle. (a) For i_{L1}. (b) For v_{C1}.

values, which is expressed as follows:

$$\begin{aligned} & i_{L1}(k+1) \\ = \; & i_{L1}(k) + d_{sh}[i_{L1\_st}(k+1) - i_{L1}(k)] \\ & +(1-d_{sh})[i_{L1\_nst}(k+1) - i_{L1}(k)] \\ = \; & i_{L1}(k) + \frac{T_S}{L_1}\left[(1-d_{sh})v_{in} - (1-2d_{sh})v_{C1}(k)\right] \end{aligned} \quad (12)$$

where d_{sh} is the ST duty cycle of the quasi-Z source, as the ratio of the action time of the ST VV to the control period in one control cycle. $i_{L1\_st}(k+1)$ refers to the predicted value of i_{L1} under the applied ST state from (3), and $i_{L1\_nst}(k+1)$ refers to the predicted value of i_{L1} under the applied NST state from (3). For the QZSI-PMSM system, the following conditions must be satisfied for stable operation to ensure that the modulation coefficients of the system are not conflicting [27]:

$$\begin{cases} 0 <= d_{sh} < 0.5 \\ 0 <= M + d_{sh} <= 1 \end{cases} \quad (13)$$

where M is the modulation ratio of the system output voltage, as the ratio of the amplitude of the output voltage to 2/3 times the DC bus voltage (V_{dc}).

Similar to i_{L1}, if the driving pulse is generated by alternating ST and NST VVs in one control cycle, the predicted value of v_{C1} in the next control cycle no longer satisfies (4). It can be assumed that v_{C1} varies linearly under the action of a single VV alone in the same control cycle as shown in Fig. 4(b). Then, the predicted value of v_{C1} under the alternating action of multiple VVs can be obtained by summing up its changing values, which is expressed as follows:

$$\begin{aligned} v_{C1}(k+1) \; = \; & v_{C1}(k) + d_{sh}[v_{C1\_st}(k+1) - v_{C1}(k)] \\ & +(1-d_{sh})[v_{C1\_nst}(k+1) - v_{C1}(k)] \\ = \; & v_{C1}(k) + \frac{T_S}{C_1}[(1-2d_{sh})i_{L1}(k+1) \\ & -(1-d_{sh})i_{dc}(k+1)] \end{aligned} \quad (14)$$

where $v_{C1\_st}(k+1)$ refers to the predicted value of v_{C1} in the applied ST state from (4), and $v_{C1\_nst}(k+1)$ refers to the predicted value of v_{C1} in the applied NST state from (4). This equation contains the constant terms related to the system parameters, the acquisition variable v_{C1} at the current moment, the predicted value $i_{L1}(k+1)$ that can be derived from (12), d_{sh} that can be derived from (15), and the predicted value of the dc bus current for the next control cycle, $i_{dc}(k+1)$. Since different NST VVs correspond to different switching states, it can be analyzed from (5) that $i_{dc}(k+1)$ takes different values when different NST VVs are applied in the same sampling period. Therefore, the problem of controlling the predicted value of capacitor voltage $v_{C1}(k+1)$ can be equivalently converted to controlling the predicted value of dc bus current $i_{dc}(k+1)$.

The ones in (9) are constant terms related to the system parameters and the collected values of the control variables at the current moment except for the output voltage (v_d, v_q) which is an unknown quantity at the current moment. Therefore, the problem of controlling the predicted value of PMSM output current $i_{dq}(k+1)$ can be equivalently converted to controlling the predicted value of output voltage $v_{dq}(k+1)$.

In summary, the deadbeat control for i_{dq} of PMSM can be equated to the deadbeat control of v_{dq}, and the deadbeat control for v_{C1} of QZSI can be equated to the deadbeat control of i_{dc}. The predicted values of both v_{dq} and i_{dc} are related to the state of the three-phase switch of the inverter, and controlling the state of the three-phase switch can realize the control of variables on both sides of the inverter and motor.

4.2. The Calculation and Primary Correction of d_{sh} and Three-Phase Duty Cycle

ST states include single-phase ST, two-phase ST, and three-phase ST. When QZSI-PMSM applies ST VV, the switching devices of the higher and lower bridge arms of one or more phases of the inverter conduct at the same time, and the switching states of the higher and lower bridge arms of the phase (S_{xH}, S_{xL}, $x = a, b, c$) are set to 1 at the same time. In this paper, only single-phase ST VVs are used in order to reduce the switching frequency of proposed TDCM-MPC strategy.

The three-phase, two-level QZSI can provide eight NST VVs and twelve single-phase ST VVs. The switching states (S_{aH}, S_{bH}, S_{cH}, S_{aL}, S_{bL}, S_{cL}), inverter output voltages and i_{dc} of different NST VVs are detailed in Table 1.

The goal of the deadbeat control is to make the predicted value of this control variable in the next control cycle equal

TABLE 1. Information of different NST VVs.

V_{nst}	$S_{aH}, S_{bH}, S_{cH}, S_{aL}, S_{bL}, S_{cL}$	v_{out}	$i_{dc}(k+1)$
V_0	$(0,0,0,1,1,1)$	0	0
V_1	$(1,0,0,0,1,1)$	$2V_{dc}/3$	i_a
V_2	$(1,1,0,0,0,1)$	$V_{dc}/3+j\sqrt{3}V_{dc}/3$	i_a+i_b
V_3	$(0,1,0,1,0,1)$	$-V_{dc}/3+j\sqrt{3}V_{dc}/3$	i_b
V_4	$(0,1,1,1,0,0)$	$-2V_{dc}/3$	i_b+i_c
V_5	$(0,0,1,1,1,0)$	$-V_{dc}/3-j\sqrt{3}V_{dc}/3$	i_c
V_6	$(1,0,1,0,1,0)$	$V_{dc}/3-j\sqrt{3}V_{dc}/3$	i_a+i_c
V_7	$(1,1,1,0,0,0)$	0	0

to its reference value. The calculated value of d_{sh} can be obtained by directly applying the deadbeat control to i_{L1} by reverting (12):

$$d_{sh}=\frac{[i_{L1\_ref}-i_{L1}(k)]L_1/T_S+v_{C1}(k)-v_{in}}{2v_{C1}(k)-v_{in}} \tag{15}$$

The calculated value of d_{sh} fluctuates greatly when the operating conditions change suddenly, and it may no longer meet the stable operation conditions of (13) at this time, so it is necessary to correct it. When the value of d_{sh} is less than 0, make it equal to 0; when the value of d_{sh} is greater than 0.5, make it equal to 0.5.

Due to the characteristic of $i_a+i_b+i_c=0$ for three-phase currents, it can be summarized from Table 1 that the action of any NST VVs on $i_{dc}(k+1)$ can be replaced completely by the joint action of its two adjacent NST VVs in equal time. Taking V_3 as an example, the predicted value of i_{dc} under its action is i_b. Its two adjacent NST VVs are V_2 and V_4, and the predicted values of i_{dc} under its action are i_a+i_b and i_b+i_c, respectively. If V_2 and V_4 act jointly at the same time, the predicted value of i_{dc} is $i_a+2i_b+i_c$, which is equivalent to i_b due to the characteristic of $i_a+i_b+i_c=0$. The predicted value of v_{C1} under applying multiple VVs in one control cycle is shown in (14), and the reference value of the DC bus current can be obtained by applying deadbeat control directly to it as follows:

$$i_{dc\_ref}=\frac{(1-2d_{sh})i_{L1}(k+1)-[v_{C1\_ref}-v_{C1}(k)]C_1/T_S}{1-d_{sh}} \tag{16}$$

If multiple NST VVs are applied in one control cycle, the predicted value of i_{dc} when applying NST state no longer satisfies (5). The predicted value of average i_{dc} when applying NST state in a control cycle is defined as follows:

$$\overline{i_{dc}}(k+1)=d_ai_a+d_bi_b+d_ci_c \tag{17}$$

where d_a, d_b, and d_c are the duty cycles of *abc* three-phase, respectively, which are the ratios of the inverter three-phase higher bridge arm turn-on and lower bridge arm turn-off time to the whole control cycle. The states of each phase are independent of each other, and the voltage acting on the load satisfies the principle of superposition and also satisfies the vector synthesis relationship in terms of space vectors [30]. For the voltage source inverter (VSI), the three-phase duty cycle shall be satisfied as:

$$0<=d_a,d_b,d_c<=1 \tag{18}$$

From (4), the predicted value of v_{C1} in ST state is independent of i_{dc}. For QZSI drive systems, it is commonly necessary to insert ST VVs into NST VVs. To facilitate modulation of the voltage vector, d_{sh} can be stripped out beforehand, and the three-phase duty cycle at this time should satisfy the following condition:

$$0<=d_a,d_b,d_c<=1-d_{sh} \tag{19}$$

The reference value of v_{dq} is obtained by applying deadbeat control directly to i_{dq} by reverting (9):

$$\begin{cases} v_{d\_ref}=\frac{L_d}{T_S}\left[i_{d\_ref}-(1-\frac{R_sT_s}{L_d})i_d(k)-\frac{T_s\omega_eL_qi_q(k)}{L_d}\right] \\ v_{q\_ref}=\frac{L_q}{T_S}\left[i_{q\_ref}-(1-\frac{R_sT_s}{L_q})i_q(k)+\frac{T_s\omega_eL_di_d(k)+T_s\omega_e\psi_f}{L_q}\right] \end{cases} \tag{20}$$

Convert the reference value of v_{dq} to the two-phase stationary coordinate system:

$$\begin{cases} v_{\alpha\_ref}=v_{d\_ref}\cos\theta-v_{q\_ref}\sin\theta \\ v_{\beta\_ref}=v_{d\_ref}\sin\theta+v_{q\_ref}\cos\theta \end{cases} \tag{21}$$

Similar to the average i_{dc}, the reference value of output voltage can be presented in the form of three-phase duty cycle. Create a matrix as follows:

$$\begin{bmatrix} V_{1\alpha} & V_{3\alpha} & V_{5\alpha} \\ V_{1\beta} & V_{3\beta} & V_{5\beta} \\ i_a & i_b & i_c \end{bmatrix}\begin{bmatrix} d_a \\ d_b \\ d_c \end{bmatrix}=\begin{bmatrix} v_{\alpha\_ref} \\ v_{\beta\_ref} \\ i_{dc\_ref} \end{bmatrix} \tag{22}$$

where $V_{1\alpha}$, $V_{1\beta}$ are the components of V_1 on the α-β axis; $V_{3\alpha}$, $V_{3\beta}$ are the components of V_3 on the α-β axis; $V_{5\alpha}$, $V_{5\beta}$ are the components of V_5 on the α-β axis.

A system of nonhomogeneous linear equations $\mathbf{Ax} = \mathbf{b}$ is shown in (22). Applying elementary row transformations to its augmented matrix and organizing them yields:

$$(A|b) \rightarrow \begin{bmatrix} 1 & 0 & -1 & \frac{3v_{\alpha\_ref}+\sqrt{3}v_{\beta\_ref}}{2V_{dc}} \\ 0 & 1 & -1 & \frac{\sqrt{3}v_{\beta\_ref}}{V_{dc}} \\ 0 & 0 & 0 & \frac{2i_{dc\_ref}}{i_b-i_c} - \frac{i_a}{i_b-i_c} \cdot \frac{3v_{\alpha\_ref}}{V_{dc}} - \frac{\sqrt{3}v_{\beta\_ref}}{V_{dc}} \end{bmatrix} \quad (23)$$

where b_3 (the element in the third row and fourth column of the above matrix) is a change term containing multiple references (i_{dc_ref}, v_{α_ref}, v_{β_ref}) and measured values (i_a, i_b, i_c) at the current moment, which takes the value 0 only in very special cases. The coefficient matrix $\mathbf{A}$ of this system of linear equations has rank 2, and the augmentation matrix ($\mathbf{A}|\mathbf{b}$) has rank 3 (except in very special cases). Therefore, there is no solution to this system of linear equations, so other methods of calculating the three-phase duty cycle can only be considered.

Consider that v_{C1} is the outer loop of QZSI and that its fluctuation is small, while i_{dq} is the inner loop of PMSM, and its fluctuation is large. Therefore, a TDCM-MPC strategy is proposed boldly in this paper. The output voltage deadbeat control is applied preferentially to calculate three-phase duty cycle, and then three-phase duty cycle is corrected according to the capacitor voltage prediction error value.

A new system of nonhomogeneous linear equations $\mathbf{A}_1\mathbf{x}_1 = \mathbf{b}_1$ is constituted after removing all the elements of the third line of (23), and it has a general solution as:

$$\begin{aligned} &[d_a, d_b, d_c]^T \\ &= k[1,1,1]^T + [(3v_{\alpha\_ref} + \sqrt{3}v_{\beta\_ref})/2V_{dc}, \\ &\sqrt{3}v_{\beta\_ref})/V_{dc}, 0]^T \end{aligned} \quad (24)$$

where k is an arbitrary constant, and k is firstly taken to be 0 in order to facilitate the calculation. At this time, the initial value of d_c is 0, and the initial values of d_a and d_b are determined by the collection and reference value of the system in current moment. The maximum value of d_a, d_b, and d_c is labeled as $d_{\max}$, and the minimum value is labeled as $d_{\min}$:

$$d_{\max} = \max\{d_a, d_b, d_c\}, d_{\min} = \min\{d_a, d_b, d_c\} \quad (25)$$

The first correction for three-phase duty cycle is performed according to (19) as follows:

1) Judge whether three-phase duty cycle has a negative value (whether $d_{\min}$ is less than 0). Since it has been determined that $d_{\min}$ is a non-positive value, the minimum value of three-phase duty cycle can be directly corrected to 0 by the following operation regardless of its value: let $d_{a1} = d_a - d_{\min}$, $d_{b1} = d_b - d_{\min}$, and $d_{c1} = d_c - d_{\min}$. (This correction does not affect the amplitude and direction of v_{dq} or the magnitude of i_{dc}.)

2) Judge whether three-phase duty cycle is over-regulated (whether $d_{\max}$-$d_{\min}$ is greater than $1 - d_{sh}$). If the judgment is no, directly output: $d_{a2} = d_{a1}$, $d_{b2} = d_{b1}$, $d_{c2} = d_{c1}$; if the judgment is yes, three-phase duty cycle can be corrected by the following operation overshoot: let $d_{a2} = d_{a1} * (1 - d_{sh})/(d_{\max} - d_{\min})$, $d_{b2} = d_{b1} * (1 - d_{sh})/(d_{\max} - d_{\min})$, $d_{c2} = d_{c1} * (1 - d_{sh})/(d_{\max} - d_{\min})$. (This correction action does not affect the direction of v_{dq}, but it does affect the amplitude of v_{dq} and the magnitude of i_{dc}.)

4.3. The Secondary Correction of Three-Phase Duty Cycle

The d_{a2}, d_{b2}, and d_{c2} obtained in Section 4.2 of this paper are able to minimize the error of PMSM output current. However, the matching of the predicted value corresponding to (17) with the reference value corresponding to (16) has not yet been considered at this point. Therefore, it is necessary to perform a secondary correction of three-phase duty cycle based on the prediction error of v_{C1} to minimize the overall error of QZSI-PMSM system.

A correction threshold ξ is defined firstly, and the secondary correction of three-phase duty cycle is triggered as an action only when the error ($|v_{C1}(k+1) - v_{C1\_ref}|$) exceeds it. If the correction is carried out in full accordance with the realization of deadbeat control for v_{C1}, there will be a large deviation from the calculation results in Section 4.2, which is not desirable. Therefore, only a certain proportion of correction can be made to d_{a2}, d_{b2}, and d_{c2}, and the correction ratio is defined as D. The corrected reference value of i_{dc} can be calculated by the following formula:

$$i^D_{dc\_ref} = Di_{dc\_ref} + (1-D)\overline{i_{dc}}(k+1) \quad (26)$$

At least one of d_{a2}, d_{b2}, and d_{c2} is 0, and the rest are positive. Record the phase with minimum duty cycle as X and the phase with maximum duty cycle as Z, while the other one is recorded as Y. In the proposed algorithm, the duty cycle of X phase is prioritized to keep unchanged, while the duty cycles of the other two phases (Y, Z) are needed to be corrected, and the their correction values are equal. The corrected reference value of i_{dc} can also be expressed by the following formula:

$$i^D_{dc\_ref} = d_X i_X + (d_Y + d_D) i_Y + (d_Z + d_D) i_Z \quad (27)$$

where d_D is the secondary correction value of three-phase duty cycle. It can be obtained by coupling with (17) and (27):

$$d_D = \frac{i^D_{dc\_ref} - \overline{i_{dc}}(k+1)}{i_Y + i_Z} = \frac{\overline{i_{dc}}(k+1) - i^D_{dc\_ref}}{i_X} \quad (28)$$

The three-phase duty cycle after the secondary correction can be obtained as follows:

1) If $d_X = d_{a2}$, then $d_{a3} = d_{a2}$, $d_{b3} = d_{b2} + d_D$, $d_{c3} = d_{c2} + d_D$.

2) If $d_X = d_{b2}$, then $d_{a3} = d_{a2} + d_D$, $d_{b3} = d_{b2}$, $d_{c3} = d_{c2} + d_D$.

3) If $d_X = d_{c2}$, then $d_{a3} = d_{a2} + d_D$, $d_{b3} = d_{b2} + d_D$, $d_{c3} = d_{c2}$.

However, the secondary correction value may be overshooting if the calculated value of d_{a2}, d_{b2}, d_{c2} is large, and the value of d_D is greater than 0. Therefore, repeat the action of correcting overshoot in Section 4.2 to get d_{a4}, d_{b4}, and d_{c4}.

4.4. The Output of Driving Pulse

The values of d_{a4}, d_{b4}, and d_{c4} obtained in Section 4.3 may be different from each other, but they all satisfy (19) at the same

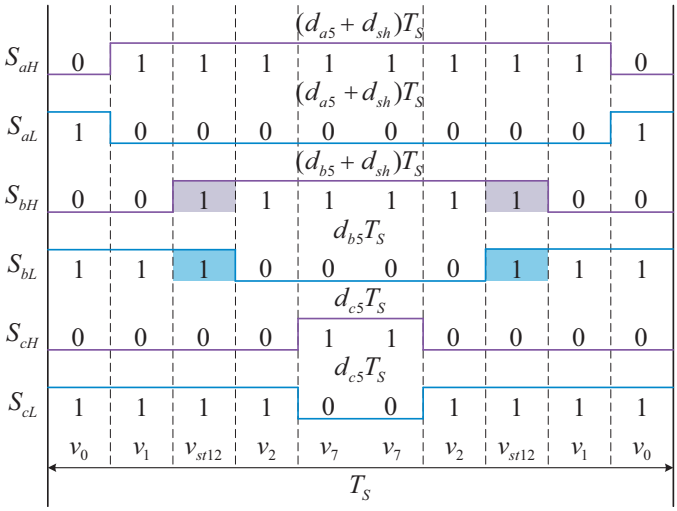

FIGURE 5. The diagram of driving pulse.

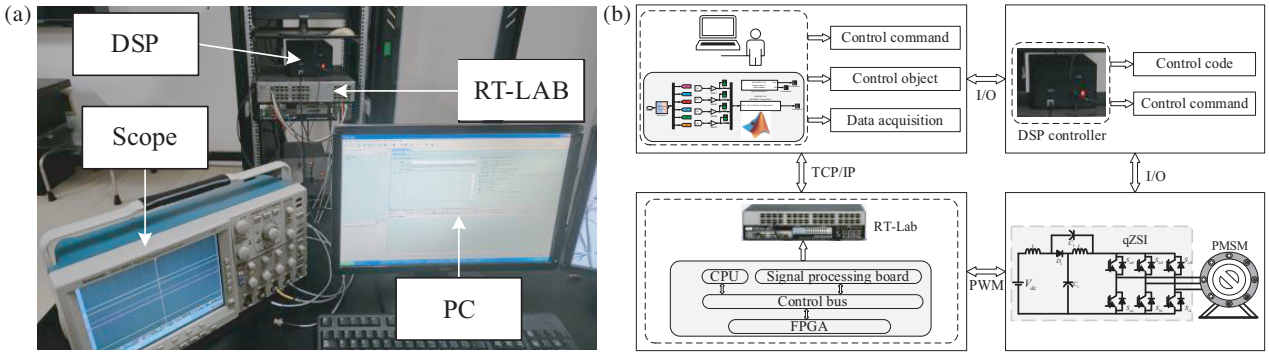

FIGURE 6. Experimental platform. (a) RT-LAB experimental platform. (b) RT-LAB in-the-loop system configuration.

time. To obtain better control performance, the two zero VVs (v_0 and v_7) can be made to act for equal time, and the updated three-phase duty cycles are shown below:

$$\begin{cases} d_{a5} = d_{a4} + [(1 - d_{sh} - \max(d_{a4}, d_{b4}, d_{c4})]/2 \\ d_{b5} = d_{b4} + [(1 - d_{sh} - \max(d_{a4}, d_{b4}, d_{c4})]/2 \\ d_{c5} = d_{c4} + [(1 - d_{sh} - \max(d_{a4}, d_{b4}, d_{c4})]/2 \end{cases} \tag{29}$$

In Section 4.2, d_{sh} has been separated in preparation for vector modulation. In the proposed strategy, the ST VVs are inserted into the NST VVs by adding d_{sh} to three-phase duty cycle. The duty cycle of the three-phase upper and lower bridge arms is adjusted as follows:

$$\begin{cases} d_{XH} = d_X \\ d_{XL} = d_X \\ d_{YH} = d_Y + d_{sh} \\ d_{YL} = d_Y \\ d_{ZH} = d_Z + d_{sh} \\ d_{ZL} = d_Z + d_{sh} \end{cases} \tag{30}$$

where d_X, d_Y, and d_Z still satisfy $d_X < d_Y < d_Z$. The subscript H indicates the upper bridge arm of the inverter bridge, and the subscript L indicates the lower bridge arm of the inverter bridge.

Taking $d_{a5} > d_{b5} > d_{c5}$ as an example, the output voltage of this control cycle is in the first sector. The drive pulses are generated by the joint work of zero VVs v_0 and v_7, the effective VVs v_1 and v_2, and the single-phase ST VV v_{st}, as shown in Fig. 5.

5. EXPERIMENTAL VERIFICATION

In order to demonstrate the effectiveness and superiority of the proposed TDCM-MPC strategy, an experimental model is constructed and validated on an RT-LAB semi-physical experimental platform. The RT-LAB experimental platform and in-the-loop system configuration are shown in Fig. 6, where the digital signal processing (DSP) adopts TMS320F2812. The parameters of QZSI-PMSM system are shown in Table 2. The K_p and K_i of the PMSM speed control loop are set to 12 and 200, respectively, while those of the QZSI capacitive voltage control loop are set to 0.95 and 50, respectively. The weight coefficients in (11) are set to 188, 1, and 0.12, respectively, which are obtained through repeated experiments. In addition, the proposed TDCM-MPC strategy keeps the number of switching times unchanged at 6 times in one control cycle, while the conventional FCS-MPC strategy has switching times ranging from 0 to 2 in one control cycle and needs to be switched to

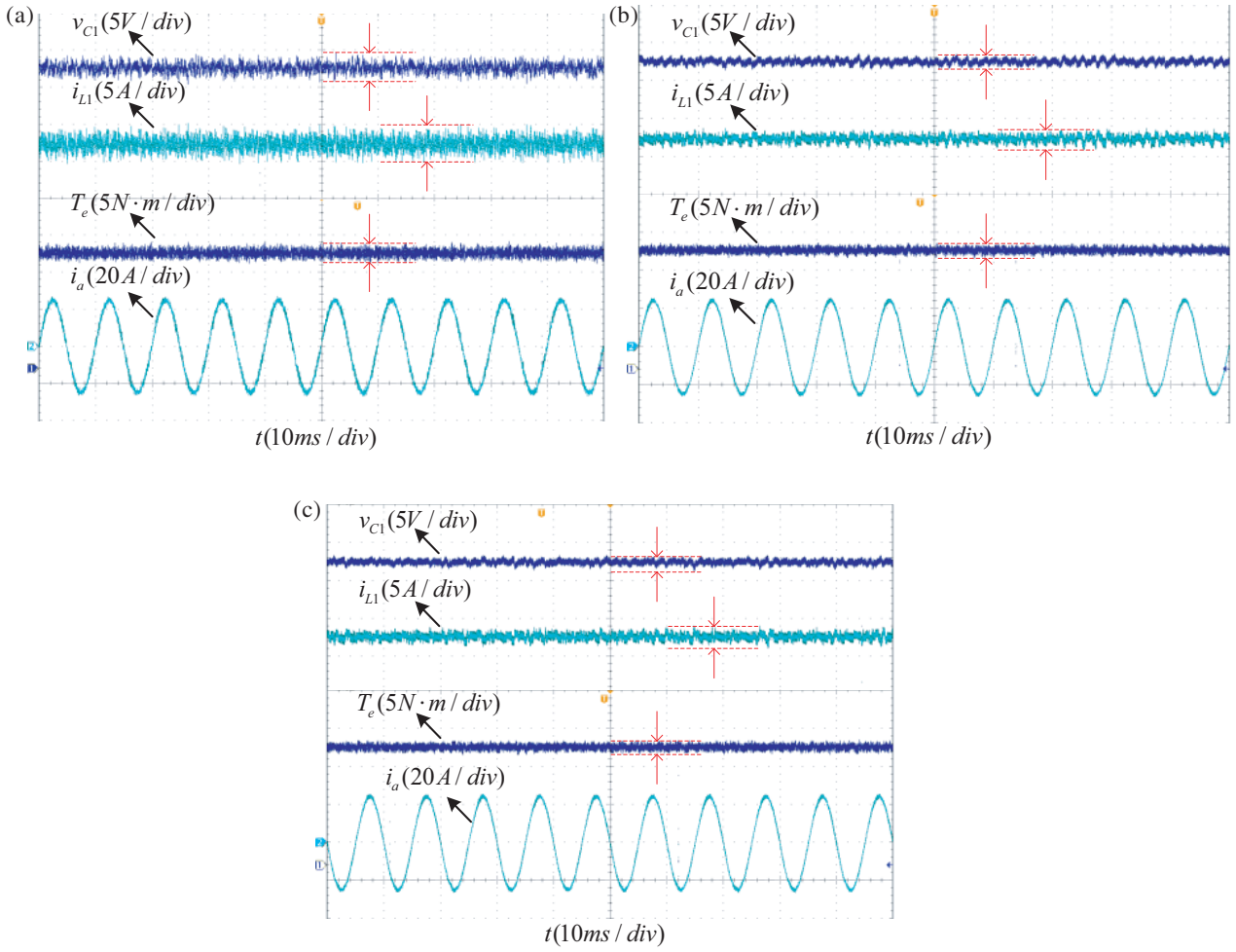

FIGURE 7. The experimental waveforms of steady-state under different strategies. (a) FCS-MPC strategy. (b) TDCM-MPC strategy. (c) TDCM-MPC strategy (without secondary correction).

TABLE 2. Parameters of QZSI and PMSM.

Parameter	Value	Unit
Number of pole pairs	4	/
Stator resistance	0.15	Ω
Stator inductance	1.625	mH
Permanent magnet flux	0.1	Wb
Moment of inertia	4.78	$g\cdot cm^2$
Rated speed	2000	r/min
Rated torque	15	$N\cdot m$
Z-Source Capacitor	470	μF
Z-Source Inductor	3	mH
DC power supply	180	V

three-phase ST state frequently. In order to make the average switching frequency of the two control strategies in the experiment basically the same, the control period of the TDCM-MPC strategy is set to 100 μs while the control period of the FCS-MPC strategy is set to 21 μs.

5.1. Comparative Experiments on Steady-state Effects

The selection of correction threshold ξ and correction ratio D depends on the operating conditions of QZSI-PMSM system (including load torque, motor speed, and capacitor voltage reference). In the experiments of this paper, they are set to 0.4 and 0.15, respectively. The values are obtained by repeated experiments, which can compare the effects of proposed strategy clearly and explicitly.

In the first experiment, the reference value of v_{C1} is given as 240 V. The operation of QZSI-PMSM is tested at a working condition of 1500 r/min speed with 15 $N\cdot m$ load torque. The steady-state experimental waveforms for both control strategies are presented in Fig. 7. It can be observed from Fig. 7(a) that there are large fluctuations in the inductor current, capacitor voltage, and torque when the FCS-MPC strategy is adopted. The control effect is significantly optimized by the proposed TDCM-MPC strategy with basically the same switching frequency. The superiority of proposed TDCM-MPC strategy is more visually demonstrated in Table 3.

The experimental results of the TDCM-MPC strategy when D is taken as 0 are also shown in Table 3 and Fig. 7(c). At this time, the control system omits the action of secondary correc-

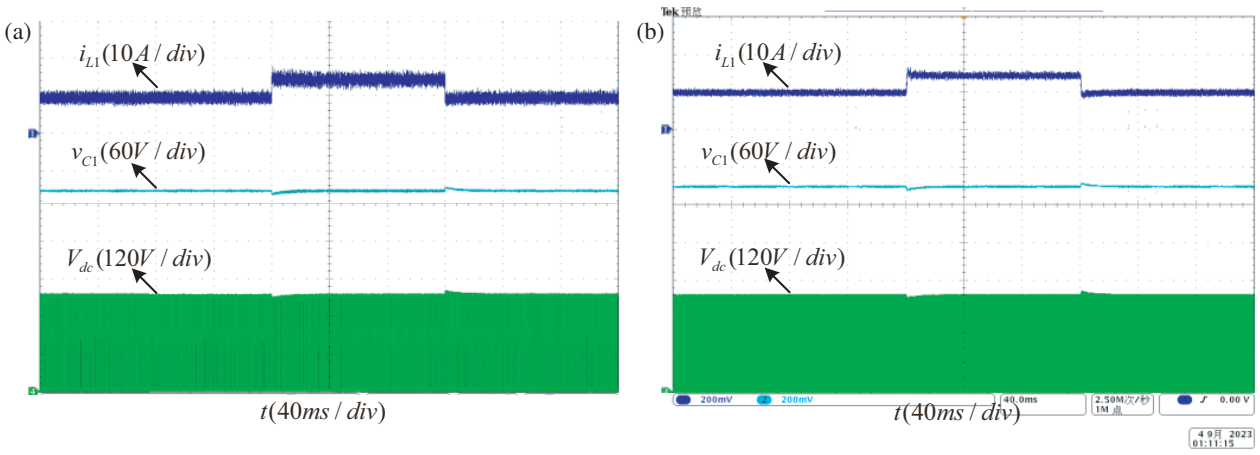

FIGURE 8. The experimental waveforms of QZSI at variable load torque. (a) FCS-MPC strategy. (b) TDCM-MPC strategy.

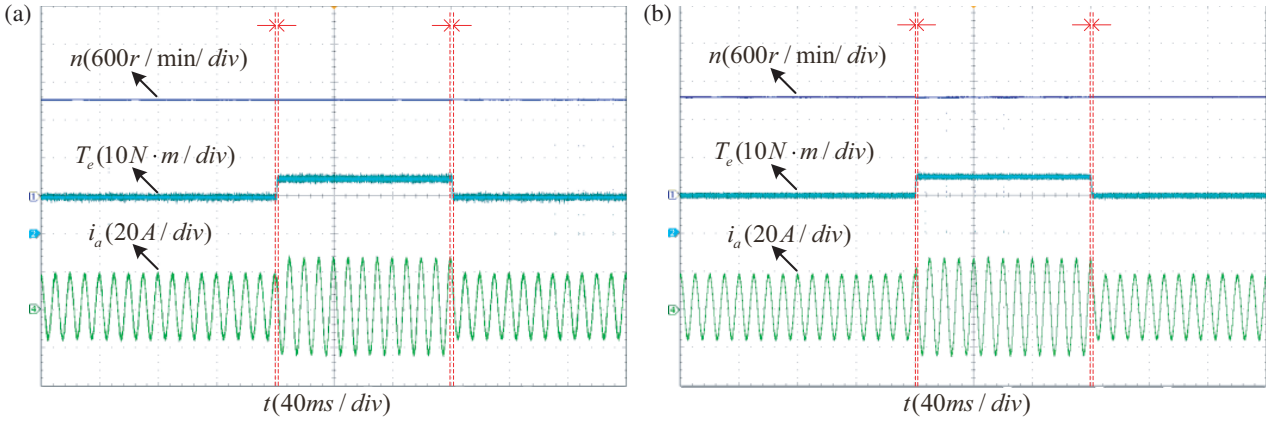

FIGURE 9. The experimental waveforms of PMSM at variable load torque. (a) FCS-MPC strategy. (b) TDCM-MPC strategy.

TABLE 3. Steady-state experimental results of multiple control variables.

control variables	7(a)	7(b)	optimisation rate (%)	7(c)
Δv_{C1} (V)	3.91	2.01	48.59	2.17
Δi_{L1} (A)	4.98	2.66	46.58	2.78
ΔT_e (N · m)	2.59	2.05	20.85	1.95
i_a THD(%)	2.87	2.11	26.48	2.04

tion. Comparing Fig. 7(b) with Fig. 7(c), it can be seen that when the secondary correction is applied to the control system, the steady-state ripples of v_{C1} and i_{L1} decrease while the steady-state ripple of torque and the THD of i_a increase. At this point, the controllable variables expand from three (i_{L1}, i_d, and i_q) to four (v_{C1}, i_{L1}, i_d, and i_q), which is consistent with the theoretical analysis in Section 4.3. Therefore, the correctness of the system of equations demonstrated in (22) is proved, and the overall control of four control variables can be realized in the proposed TDCM-MPC strategy.

5.2. Comparative Experiments on Dynamic Effects

After comparing the steady-state performances of both control strategies, their dynamic performances are compared when the load torque changes. The reference value of v_{C1} is set to 240 V, the reference value of motor speed set to 1500 r/min, and the motor load is sequentially stepped from 10 N · m to 15 N · m and from 15 N · m to 10 N · m. It can be seen from Fig. 9 that the proposed TDCM-MPC strategy can obtain similar dynamic performance to the conventional FCS-MPC. In particular, when the torque is stepped from 10 N · m to 15 N · m, both strategies can quickly track its reference value in about 2.0 ms, and when the torque is stepped from 15 N · m to 10 N · m, both strategies can quickly track its reference value in about 2.4 ms. It can be seen from Fig. 8 that the dynamic response for i_{L1} of QZSI is consistent with the motor load under both control strategies.

In addition, the dynamic responses of both strategies are compared when motor speed changes. The reference value of v_{C1} is set to 240 V, the motor load kept constant at 15 N · m, and the reference value of motor speed is sequentially increased from 1500 r/min to 1800 r/min and decreased from 1800 r/min to 1500 r/min. It can be seen from Fig. 11 that there is a slight difference in the dynamic performance of both control strategies. When the reference value of motor speed is increased from 1500 r/min to 1800 r/min, the response time of FCS-MPC is about 22 ms, while the response time of TDCM-MPC is about 40 ms. When the reference value of motor speed decreases from 1800 r/min to 1500 r/min, the response time of FCS-MPC

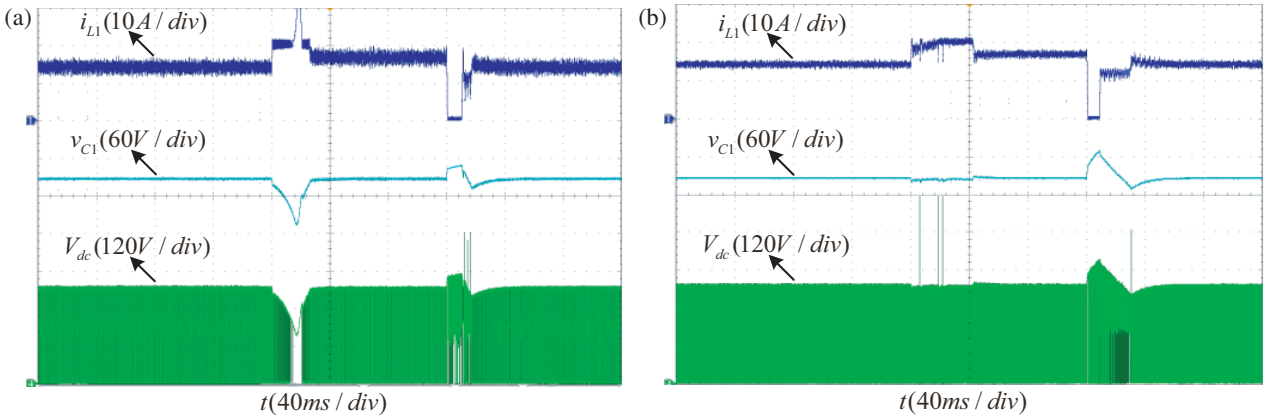

FIGURE 10. The experimental waveforms of QZSI at variable speed. (a) FCS-MPC strategy. (b) TDCM-MPC strategy.

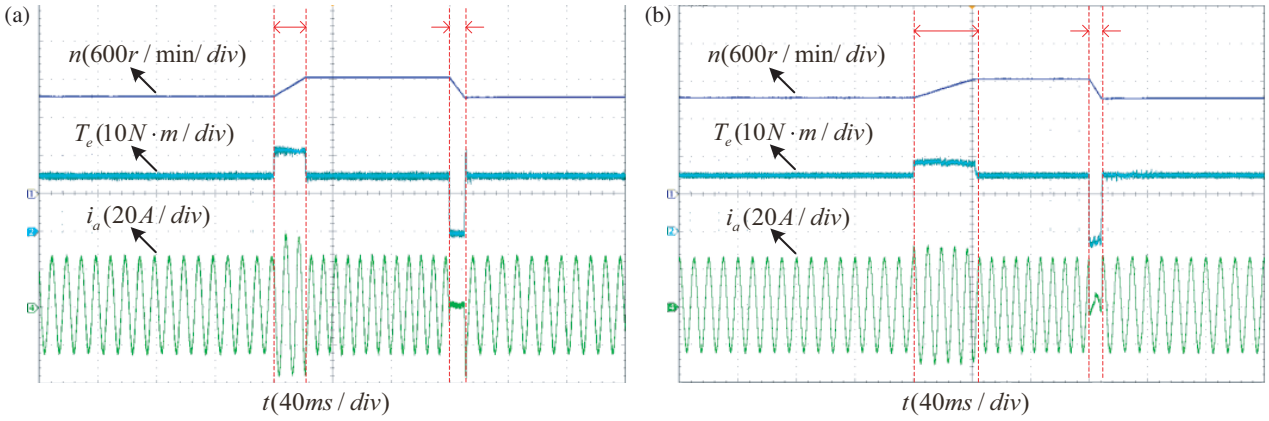

FIGURE 11. The experimental waveforms of PMSM at variable speed. (a) FCS-MPC strategy. (b) TDCM-MPC strategy.

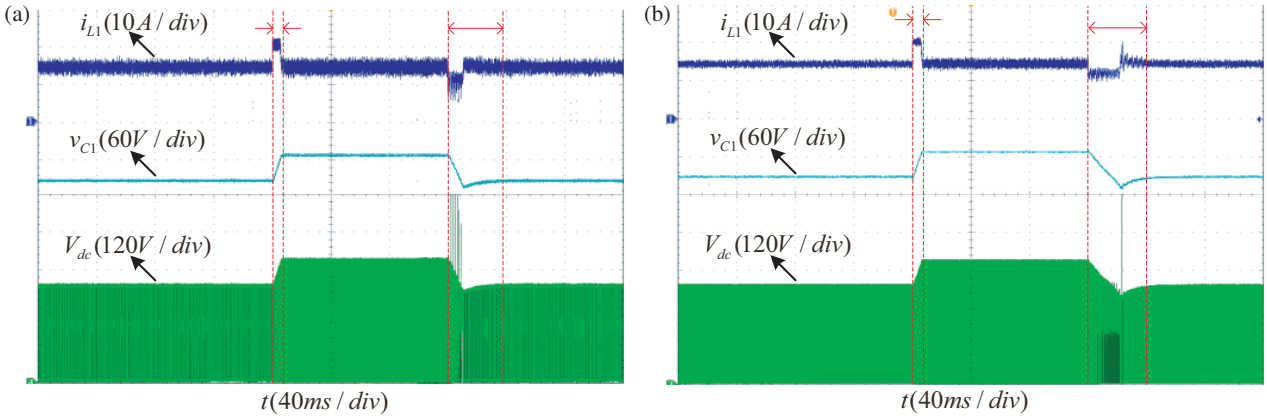

FIGURE 12. The experimental waveforms of QZSI at variable DC bus voltage. (a) FCS-MPC strategy. (b) TDCM-MPC strategy.

is about 11.4 ms, while the response time of TDCM-MPC is about 9.5 ms. This is due to the different basic logics of the two algorithms, as shown in Fig. 10, when the motor speed increases, the capacitor voltage under the FCS-MPC strategy will deviate from the reference value to a large extent to speed up the dynamic response to the motor speed, whereas the capacitor voltage under the proposed TDCM-MPC strategy will strictly follow its reference value, which will result in a slower dynamic response of the system to the motor speed. In this case, a large transient value of inductor current is present as shown in Fig. 10(a). This situation may cause damage to the inductor in actual application, which is another drawback of the conventional strategy. On the contrary, the proposed TDCM-MPC

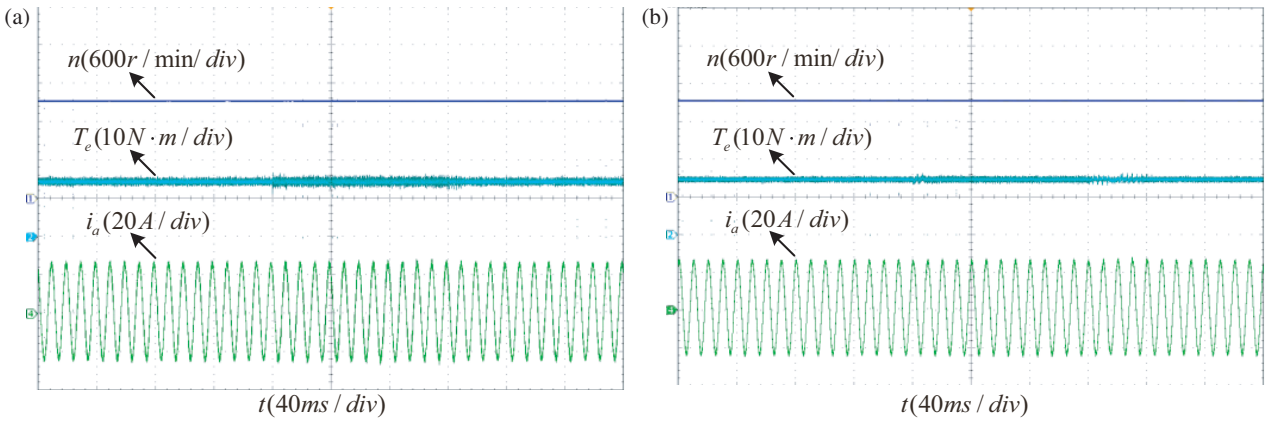

FIGURE 13. The experimental waveforms of PMSM at variable DC bus voltage. (a) FCS-MPC strategy. (b) TDCM-MPC strategy.

strategy is able to avoid such problems thanks to its duty cycle correction.

Finally, the dynamic responses of both strategies are compared when DC bus voltage changes. The motor load is kept constant at 15 N · m; the reference value of the motor speed is kept constant at 1500 r/min; the reference value of v_{C1} rises from 240 V to 280 V and decreases from 280 V to 240 V; and the corresponding DC bus voltage at the output of the inverter increases from 300 V to 380 V and decreases from 380 V to 300 V. It can be seen from Fig. 12 that the proposed TDCM-MPC strategy can obtain similar dynamic performance to the conventional FCS-MPC. In particular, when the DC bus voltage increases from 300 V to 380 V, both strategies can quickly track their reference values in about 7 ms, and when the torque decreases from 380 V to 300 V, both strategies can quickly track their reference values in about 39 ms. It can be seen from Fig. 13 that the motor-side control variables under both control strategies have a slight dynamic response only at the moment when the DC bus voltage changes.

The results of the above experiments are summarized in detail in Table 4.

TABLE 4. The response time of both strategies under different dynamic variations.

Dynamic changes	FCS-MPC	TDCM-MPC
T_e (10 → 15 N · m)	2.05 ms	1.92 ms
T_e (15 → 10 N · m)	2.44 ms	2.33 ms
n (1500 → 1800 r/min)	21.95 ms	40.27 ms
n (1800 → 1500 r/min)	11.37 ms	9.49 ms
v_{C1} (240 → 280 V)	7.05 ms	7.26 ms
v_{C1} (280 → 240 V)	37.51 ms	39.89 ms

Different control strategies are summarized in Table 5. It can be seen that the switching frequencies of the two control strategies are almost the same, and the proposed strategy has a shorter code execution time and fewer predictions. In addition, the construction of cost function and the design of weighting coefficients are not required in the proposed strategy.

TABLE 5. The summary of different strategies.

Control strategies	FCS-MPC	TDCM-MPC
Code execution time	0.053 ms	0.044 ms
Switching frequency	10.12 kHz	10 kHz
prediction times	8	1
weighting coefficients	3	/

6. CONCLUSION

To reduce the computational effort of FCS-MPC strategy and realize the overall control of all control variables in QZSI-PMSM system, the TDCM-MPC strategy without cost function is proposed. It can be concluded that the proposed method has the following advantages verified by theoretical analysis and experiments:

1) Multiple NST VVs and ST VV are employed to act alternately to generate the driving pulses in one control cycle. Compared with the conventional FCS-MPC method while keeping the switching frequencies approximately equal, the steady-state ripple of v_{C1}, i_{L1}, T_e and THD of i_a can be significantly reduced: in our tests, we obtain reduction by 20% up to 50%.

2) The three-phase duty cycles are calculated directly without constructing a cost function to search for optimization. Compared with the conventional FCS-MPC method, the prediction times are reduced from eight to one, and the code execution time is reduced by 17%.

3) The secondary correction is able to reduce the ripple of v_{C1}, which proves that the overall control of four control variables can be realized in proposed TDCM-MPC strategy.

ACKNOWLEDGEMENT

This work was supported by the Natural Science Foundation of Hunan Province of China under Grant Number 2023JJ50191.

REFERENCES

[1] Peng, F. Z., "Z-source inverter," *IEEE Transactions on Industry Applications*, Vol. 39, No. 2, 504–510, Mar.-Apr. 2003.

[2] Liu, Y., B. Ge, H. Abu-Rub, and F. Z. Peng, "Overview of space vector modulations for three-phase Z-source/quasi-Z-source inverters," *IEEE Transactions on Power Electronics*, Vol. 29, No. 4, 2098–2108, Apr. 2014.

[3] Ahmed, H. F., H. Cha, S.-H. Kim, and H.-G. Kim, "Switched-coupled-inductor quasi-Z-source inverter," *IEEE Transactions on Power Electronics*, Vol. 31, No. 2, 1241–1254, Feb. 2016.

[4] Noroozi, N. and M. R. Zolghadri, "Three-phase quasi-Z-source inverter with constant common-mode voltage for photovoltaic application," *IEEE Transactions on Industrial Electronics*, Vol. 65, No. 6, 4790–4798, Jun. 2018.

[5] Manoj, P., A. Kirubakaran, and V. T. Somasekhar, "An asymmetrical dual quasi-Z-source based 7-level inverter for PV applications," *IEEE Transactions on Energy Conversion*, Vol. 38, No. 2, 1097–1107, Jun. 2023.

[6] Gu, Y., Y. Chen, and B. Zhang, "Enhanced-boost quasi-Z-source inverter with an active switched Z-network," *IEEE Transactions on Industrial Electronics*, Vol. 65, No. 10, 8372–8381, Oct. 2018.

[7] Young, H. A., M. A. Perez, J. Rodriguez, and H. Abu-Rub, "Assessing finite-control-set model predictive control: A comparison with a linear current controller in two-level voltage source inverters," *IEEE Industrial Electronics Magazine*, Vol. 8, No. 1, 44–52, Mar. 2014.

[8] Dong, Q., B. Wang, L. Xia, Y. Yu, M. Tian, and D. Xu, "A virtual voltage field-weakening scheme of trajectory correction for PMSM model predictive control," *IEEE Transactions on Power Electronics*, Vol. 38, No. 3, 3044–3056, Mar. 2023.

[9] Zhang, X., C. Zhang, Z. Wang, and J. Rodríguez, "Motor-parameter-free model predictive current control for PMSM drives," *IEEE Transactions on Industrial Electronics*, Vol. 71, No. 6, 5443–5452, Jun. 2024.

[10] Bayhan, S., H. Abu-Rub, and R. S. Balog, "Model predictive control of quasi-Z-source four-leg inverter," *IEEE Transactions on Industrial Electronics*, Vol. 63, No. 7, 4506–4516, Jul. 2016.

[11] Karamanakos, P., T. Geyer, and S. Manias, "Direct voltage control of DC-DC boost converters using enumeration-based model predictive control," *IEEE Transactions on Power Electronics*, Vol. 29, No. 2, 968–978, Feb. 2014.

[12] Zhang, Y., Y. Liu, B. Luo, and Y. Ling, "Variable weight coefficient MPC control strategy for qZSI-VSG wind power grid-connected system," *IET Renewable Power Generation*, Vol. 17, No. 8, 1952–1965, 2023.

[13] Zhou, Z., C. Xia, Y. Yan, Z. Wang, and T. Shi, "Torque ripple minimization of predictive torque control for PMSM with extended control set," *IEEE Transactions on Industrial Electronics*, Vol. 64, No. 9, 6930–6939, Sep. 2017.

[14] Yuan, X., S. Zhang, and C. Zhang, "Enhanced robust deadbeat predictive current control for PMSM drives," *IEEE Access*, Vol. 7, 148 218–148 230, 2019.

[15] Zhang, X. and Y. He, "Direct voltage-selection based model predictive direct speed control for PMSM drives without weighting factor," *IEEE Transactions on Power Electronics*, Vol. 34, No. 8, 7838–7851, Aug. 2019.

[16] Li, X., Z. Xue, X. Yan, *et al.*, "Voltage vector rapid screening-based three-vector model predictive torque control for permanent magnet synchronous motor," *Transactions of China Electrotechnical Society*, Vol. 37, No. 7, 1666–1678, 2022.

[17] Liu, J., Z. Ge, X. Wu, G. Wu, S. Xiao, and K. Huang, "Predictive current control of permanent magnet synchronous motor based on duty cycle modulation," *Proceedings of the CSEE*, Vol. 40, No. 10, 3319–3327, 2020.

[18] Brosch, A., O. Wallscheid, and J. Böcker, "Long-term memory recursive least squares online identification of highly utilized permanent magnet synchronous motors for finite-control-set model predictive control," *IEEE Transactions on Power Electronics*, Vol. 38, No. 2, 1451–1467, Feb. 2023.

[19] Ramírez, R. O., J. R. Espinoza, C. R. Baier, M. Rivera, F. Villarroel, J. I. Guzman, and P. E. Melín, "Finite-state model predictive control with integral action applied to a single-phase Z-source inverter," *IEEE Journal of Emerging and Selected Topics in Power Electronics*, Vol. 7, No. 1, 228–239, Mar. 2019.

[20] Bakeer, A., M. A. Ismeil, and M. Orabi, "A powerful finite control set-model predictive control algorithm for quasi Z-source inverter," *IEEE Transactions on Industrial Informatics*, Vol. 12, No. 4, 1371–1379, Aug. 2016.

[21] Xu, Y., Y. He, and S. Li, "Logical operation-based model predictive control for quasi-Z-source inverter without weighting factor," *IEEE Journal of Emerging and Selected Topics in Power Electronics*, Vol. 9, No. 1, 1039–1051, Feb. 2021.

[22] Gannamraju, S. K. and R. Bhimasingu, "Sequential model predictive control of quasi Z-source inverter with fixed frequency operation," *International Transactions on Electrical Energy Systems*, Vol. 31, No. 11, e13068, 2021.

[23] Wu, C., J. Yang, and Q. Cheng, "Sequential-model predictive control for quasi-Z-source inverter," *Proceedings of the CSEE*, Vol. 41, No. 12, 4286–4297, 2021.

[24] Xu, Y., Y. He, H. Li, and H. Xiao, "Model predictive control using joint voltage vector for quasi-Z-source inverter with ability of suppressing current ripple," *IEEE Journal of Emerging and Selected Topics in Power Electronics*, Vol. 10, No. 1, 1108–1124, Feb. 2022.

[25] Liu, Y., H. Abu-Rub, Y. Xue, and F. Tao, "A discrete-time average model-based predictive control for a quasi-Z-source inverter," *IEEE Transactions on Industrial Electronics*, Vol. 65, No. 8, 6044–6054, Aug. 2018.

[26] Mahmoudi, H., M. Aleenejad, and R. Ahmadi, "Modulated model predictive control for a Z-source-based permanent magnet synchronous motor drive system," *IEEE Transactions on Industrial Electronics*, Vol. 65, No. 10, 8307–8319, Oct. 2018.

[27] Dong, K., T. Shi, S. Xiao, X. Li, and C. Xia, "Finite set model predictive control method for quasi-Z source inverter-permanent magnet synchronous motor drive system," *IET Electric Power Applications*, Vol. 13, No. 3, 302–309, 2019.

[28] Ahmed, A. A., A. Bakeer, H. H. Alhelou, P. Siano, and M. A. Mossa, "A new modulated finite control set-model predictive control of quasi-Z-source inverter for PMSM drives," *Electronics*, Vol. 10, No. 22, 2814, 2021.

[29] Mahmoudi, H., M. Aleenejad, and R. Ahmadi, "Torque ripple minimization for a permanent magnet synchronous motor using a modified quasi-Z-source inverter," *IEEE Transactions on Power Electronics*, Vol. 34, No. 4, 3819–3830, Apr. 2019.

[30] Sun, H. X., K. Jing, Y. Dong, *et al.*, "Research of SVPWM algorithm based on 120° coordinates system," *Transactions of China Electrotechnical Society*, Vol. 31, No. 5, 52–59, 2016.